Full Range of Wettability through Surface Modification of Single-Wall Carbon Nanotubes by Photo-Initiated Chemical Vapor Deposition

Seyedehsan Hosseininasab [a], Nathalie Faucheux [b], Gervais Soucy [b] and Jason R. Tavares [a,*]

[a] *Department of Chemical Engineering, Polytechnique Montreal, Montreal, Québec H3T 1J4, Canada*
[b] *Department of Chemical and Biotechnological Engineering, Université de Sherbrooke, Sherbrooke, Québec J1K 2R1 Canada*

ABSTRACT

Single-wall carbon nanotubes (SWCNTs) have various remarkable properties, which make them a promising candidate for many applications. However, their inherent hydrophobicity have limited their commercial use in optical, biological, and electrical applications. Photo-initiated chemical vapor deposition (PICVD) using syngas is proposed as a novel, affordable, and versatile method to tailor SWCNT wettability through the addition of oxygen-containing functional groups. Following PICVD surface treatment, X-ray photoelectron spectroscopy, water contact angle measurements (CA), thermogravimetric analysis, Raman spectroscopy and transmission electron microscopy confirm controlled oxygenation of the SWCNT surface. Indeed, this novel approach allows to reproducibly make SWCNT having surfaces properties ranging from superhydrophilic (CA<5°) to superhydrophobic (CA>150°), including any intermediate values, by simply varying operational parameters such as molar ratio of the syngas precursor, photo-polymerization time and reactor pressure (about normal conditions).

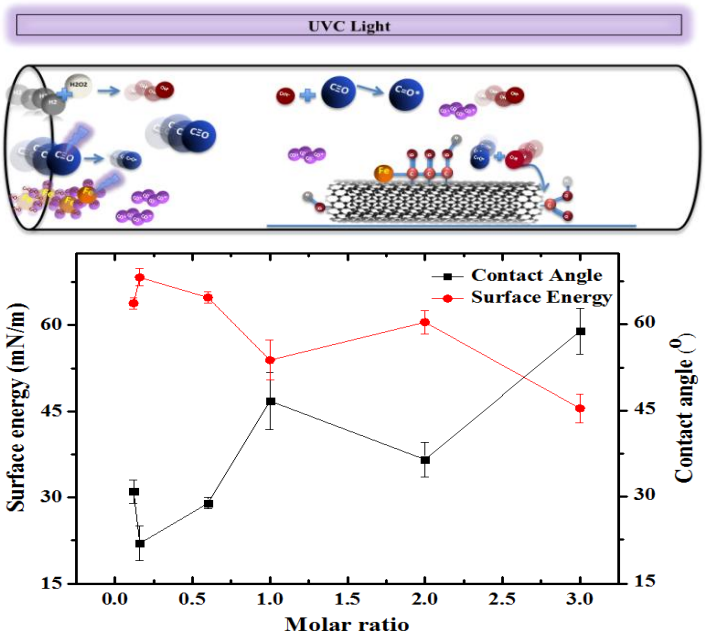

Keywords: PICVD, Surface modification, Oxygen functional group, Superhydrophilic, Superhydrophobic

* Corresponding authors: École Polytechnique de Montréal, Bureau A-554.1, C.P. 6079, Succ. Centre-Ville Montréal, Québec, Canada (H3C 3A7), Tell: +1 514 340-4711 (Ext: 2326), E-mail addresses: jason.tavares@polymtl.ca

List of abbreviations and parameters			
		S-T-SWCNT	Syngas Treated Single-Wall Carbon Nanotubes
		TACVD	Thermal Activated Chemical Vapour Deposition
		T-SWCNT	Treated Single-Wall Carbon Nanotubes
CA	Contact Angle	TEM	Transmission Electron Microscopy
DTGA	Differential Thermogravimetric Analysis	TGA	Thermogravimetric Analysis
EDS	Energy Dispersive Spectroscopy	UV	Ultra-Violet
HR	High-Resolution	XPS	X-ray Photoelectron Spectroscopy
HR-XPS	High Resolution X-ray Photoelectron Spectroscopy	γ_{sl}	Solid-Liquid Interfacial Energy
Ozone/UV	Treatment by Ozone Under UV Light	γ_l^d	Dispersive Component of Liquid Surface Tension
O-T-SWCNT	Ozone Treated Single-Wall Carbon Nanotubes	γ_l^p	Polar Component of Liquid Surface Tension
PICVD	Photo-Initiated Chemical Vapour Deposition	γ_s	Total Free Surface Tension of Solid
PECVD	Plasma Enhanced Chemical Vapour Deposition	γ_s^d	Dispersive Components of Solid Surface Tension
PI	Photo-Initiator	γ_s^p	Polar Components of Solid Surface Tension
P-SWCNT	Pure Single-Wall Carbon Nanotubes	θ	Liquid Contact Angle
SWCNT	Single-Wall Carbon Nanotubes	θ_A	Advancing Contact Angle
Syngas/PICVD	Syngas Photo-Initiated Chemical Vapour Deposition	θ_R	Receding Contact Angle

1. Introduction

Single wall carbon nanotubes (SWCNTs) have various properties of interest, such as high mechanical and electrical conductivity, remarkable thermal stability (up to 2800 °C under vacuum) [1, 2], proportionally lower weight than steel and titanium (typical materials in bone applications) [3, 4] and the highest Young's modulus among all different types of composites and nano-materials (> 1-5 TPa) [1, 4]. These individual properties make them promising candidates for a wide range of applications such as aerospace, nanocomposites, biomedical and tissue engineering, to name only a few [5-7]. These materials have also shown potential to be used in bone applications due to their similarities with triple helix collagen fibrils, in terms of size and shape (diameter of SWCNTs ranges between 0.7-1.5 nm) [8-10]. Not only can these materials enhance the mechanical properties of biomaterials [11], they can also stimulate bone regeneration [12]. Therefore, they may be effective for use in different bone substitutes, such as scaffolds and fillers.

Despite all the above-mentioned properties and potential of SWCNTs for different applications such as reinforcements in polymer nanocomposites and biomaterials synthesis, their inherent hydrophobicity and insolubility are the most challenging features that need to be addressed [2]. For example, in the case of nanocomposites, one of the most important factors that should be considered is the homogeneous dispersion of SWCNT nanofillers [7]. Untreated SWCNTs tend to aggregate due to their high surface area to volume ratio and strong van der Waals interactions while the resulting aggregation negatively overshadows mechanical, electrical and thermal properties gained by SWCNT addition [7, 13-15].

Various approaches exist to modify the CNT's surface properties and address such surface-based problems, including surfactants, oxidation, sonication and functionalization [1]. Of these, surface functionalization has been identified as a promising approach [1]. Functionalization implies the covalent grafting of a specific chemical functional group to the surface. Intuitively, the addition of oxygen-based functional groups would seem like a viable route to decrease hydrophobicity and, possibly, make them more compatible to be used in nanocomposites [7] and bio-applications [8].

Covalent functionalization, in which functional groups (such as amino and carboxylic acid groups) are grafted onto SWCNT walls, help overcome attractive forces can prevent this agglomeration and lead to better dispersion [7, 13]. Moreover, the higher reactivity of treated SWCNTs, as well as their increased interfacial bonding and load transfer with the surrounding polymer resulting from reactive functional groups (oxygen- or nitrogen-containing groups) after treatment leads to an increase in mechanical and electrical properties of nanocomposites [7]. Given the wide range of polymer materials (hydrophobic and hydrophilic) and subsequent filler-matrix interactions, a technique capable of tailoring SWCNT wettability is required.

In the case of biomedical applications, there are significant contradictions in the literature concerning the effect of such SWCNT functionalization on their cytotoxicity [16]. For example, some indicate that functionalization of SWCNTs using carboxylic acid groups reduces cell viability and proliferation [17-19], whereas Montes-Fonseca et al. (2012) reported less cytotoxicity for functionalized CNTs [20]. A deep examination of the literature reveals that the contradiction comes from different CNT properties (i.e. wettability, functional group charging, variation of SWCNT size, degree of purity and effect of surface energy, etc.) [21]. Furthermore, the contradictions regarding cell response to functionalized SWCNTs in the literature can likely be attributed to the fact that individual reports do not study surface treatments over wide ranges (i.e. no attention typically paid to the extent of functionalization) – essentially, a single treatment is applied and the cytotoxicity is analyzed [22, 23]. Beyond the issue of cytotoxicity, applications such as the selective binding of specific blood proteins (that can have polar and non-polar components) to CNTs can necessitate hydrophobic or hydrophilic surfaces [24, 25]. Therefore, before any practical biomaterial applications of CNTs can be considered, it is necessary to address the issue of surface wettability. Specifically, there is a need to study a surface modification technique capable of controlling the extent of the functionalization. Such a method should allow a "full range" of properties (from superhydrophilic to superhydrophobic, for example) using a similar reaction scheme and functional groups.

Functionalization techniques can be classified into two groups: solvent-based (wet chemistry)

and solvent-free (gas-phase) methods. Solvent-based approaches suffer from multi-step and complex preparation methodologies and can damage the CNT structure. Furthermore, separation of the treated nanomaterials from the solvent, as well as the management of solvent waste, can be a time-consuming and significant processing issue, which is generally dodged in the literature [26-30]. Gas-phase surface modification techniques can be classified according to the energy source applied for reaction initiation, including thermally activated chemical vapor deposition (TACVD) [31], plasma-enhanced CVD (PECVD) [32] and photo-initiated CVD (PICVD) [27]. Table 1 presents a detailed comparison between the current functionalization methods for CNTs.

Unlike TACVD (which uses heat, problematic for temperature-sensitive substrates) and PECVD (which requires specialized and costly plasma conditions), PICVD uses light to initiate organic deposition reactions. In this process, radicals can be generated by exposure to ultraviolet (UV) light, launching a series of heterogeneous reactions on the surface of a substrate in parallel with gas phase reactions. PICVD has been gaining interest for the surface treatment of nanomaterials because of its simple procedure, low cost, possibility of operation at or near atmospheric pressure (depending on the wavelength selected) [27, 32], higher intermolecular cross-linking [33], low energy consumption [27, 32] and, most importantly, ability to adjust the desired degree of functionalization [33].

A key parameter for PICVD is the selection of an appropriate monomer to impart the desired functional groups and surface properties (hydrophilic or hydrophobic). The selected monomer should therefore contain the desired chemical moieties, as well as contain groups capable of forming radicals following exposure to light at the selected wavelength. Ozone is a UV sensitive molecule that can be used as a precursor for oxidative attacks on SWCNTs [34]. It absorbs light significantly at 253.7 nm (peak emission in Hg discharge lamps), with an efficient quantum yield [34]. Accordingly, it can be a good precursor to treat SWCNTs under PICVD, given that Hg discharge lamps are commercially available at low cost (in the form of germicidal lamps) and light at 253.7 nm (UVC) is readily transmitted through common materials such as quartz.

Beyond oxidative attacks with ozone (which are limited to imparting hydrophilic functionalities on CNTs), it is possible to form organic coatings with UVC light, namely by using syngas as a precursor [27]. Our research team has previously demonstrated that syngas (CO and H_2) could be used in PICVD to form hydrophilic and hydrophobic surfaces on copper substrates by manipulating treatment pressure (near atmospheric) and CO/H_2 ratio [27]. In this process, radicals produced from the dissociation of a photo-initiator (PI) and the precursor mixture lead to a combination of gas phase and surface reactions to impart surface functionality [31, 32].

Surface wettability can be investigated through contact angle (CA) measurements, namely through two approaches: static and dynamic methods. Static (or "sessile drop") CA is a measure of the angle between a liquid droplet (of known polarity) and the surface of interest. This method has been applied extensively by CNT researchers - Woo et al. (2010) found that the static CA with water of CNT films oxidized at 400 °C for 30 min under air flow was 96.9° [35]. Koumoulos and Charitidis (2017) measured the static CA to assess the wettability of CNT arrays synthesized by CVD, finding values of. 136° and 150° for water and glycerol droplets, respectively [36]. Liu et al. (2017) surface treated CNT films by atmospheric pressure plasma using a mixture of helium and oxygen, leading to a static contact angle decrease from 105° to 80°, 64°, and 47° only after 0.1, 0.2, and 0.3 s treatments, respectively [37]. Indeed, oxygen plasma functionalization is a common method to make CNTs hydrophilic [38, 39] Similiarly, Wang et al (2009) measured the wettability of graphene and graphene oxide thin films, reporting surface energies of 46.7 and 62.1 mJ/m^2, respectively [40]. Alternatively, the dynamic CA assesses the angle between the liquid and the surface under moving boundaries (three phases: air, liquid and solid film). The dynamic CA is defined through three major parameters: advancing CA (θ_A), receding CA (θ_R), and CA hysteresis. θ_A indicates the wetting ability of a liquid on a solid film upon initial contact, whereas θ_R describes the difficulty of removing the liquid from the surface. CA hysteresis is defined as the difference between the two (θ_A - θ_R). Dynamic CA serves as an indicator of surface quality in terms of inhomogeneity of chemical treatment, roughness, and stability [41-43]. For example, Lau et al (2003) employed dynamic CA to investigate the stability and wettability behavior of aligned CNT forests coated by poly(tetrafluoroethylene)(to make superhydrobic surfaces through a combination of chemical and roughness changes) [44]. Aside from CA approaches, an inverse gas chromatography-surface energy analyzer (IGC-SEA) may be used to assess expected wettability [45, 46]. For example, Li et al.(2016) measured surface energy of carbon fibres coated with carbon nanotubes. They could successfully fabricate CNT coated Carbon fibres by electrospray method resulted in a multi-scale hierarchal structure without any tensile strength changes of fibres [47]. Both CA and IGC-SEA approaches applied to CNT rely on measurements of the nanomaterials in a bucky paper configuration (or deposited/grown on a surface) – in other words, in aggregate form. To measure the wettability of individual CNTs, indirect measurements must be applied, typically with the CNT in a dispersed state – these can range from stability of CNT in suspension [48] to measurements of the zeta potential (with corrections applied for high-aspect ratio particles) [49].

To the best of our knowledge, the use of syngas and PICVD (syngas/PICVD) on SWCNTs has

never been investigated, and shows potential as a viable method to systematically modify CNTs over a wide range of surface energy. Given the importance of process control and materials customization in the fields of chemical and materials engineering, we consider this exploration to be significant. Hence, the main goal of this study is the surface treatment of SWCNTs by syngas/PICVD to allow the addition of oxygen-containing functional groups and thus obtain different degrees of functionalization and, consequently, various surface energies. In this regard, syngas/PICVD is compared with an ozone/UV-based (ozone/UV) treatment.

Table 1. Comparison between some common functionalization methods of nanoparticles and carbon nanotubes

Methods	Type	Advantages	Drawbacks	Ref.
Wet chemistry	Covalent (liquid phase)	1- Easy scale-up 2- Facile control of the extent of hydrophilicity 3- Potentially low-cost method (depending on reagents)	1- Multi-step process 2- Unable to make and control extend of hydrophobicity 3- Time consuming 4- Solvent waste management 5- Destructive method for hexagonal structure of CNTs 6- Specific complex reagents for the functionalization	[27-29]
Surfactants	Non-covalent	1- Able to make both hydrophilic and hydrophobic surfaces (with different or amphiphilic molecules) 2- Non-destructive method for the hexagonal structure of CNTs 3- Preserves the mechanical and electrical properties of SWCNTs	1- Low stability due to weak binding forces 2- Extended sonication period required 3- Poor scale reliability	[50-52]
TACVD	Covalent (gas-phase)	1- Large scale treatment 2- Able to make and control extend of functionality 3- High deposition rates and conversions	1- Vacuum requirement 2- High temperature requirement 3- Lack of appropriate range of monomers 4- Expensive (processing and capital costs) 5- Poor energy efficiency 6- Destructive method for the hexagonal structure of CNTs 7- Difficult to make hydrophobic surfaces	[28, 31]
PECVD	Covalent (gas-phase)	1- Large scale treatment (atmospheric discharges) 2- Able to make and control extend of functionality 3- High deposition rates and conversion 4- Control on deposition temperature	1- Expensive (processing and capital costs, specialized operation) 2- Unreacted precursors and by-products, often embedded in functional coating 3- Low efficiency because of the energy wasted on low energy electrons 4- Unstructured coatings with low cross-linking 5- Limited to small scales for low-pressure discharges	[31, 48, 53-55]
PICVD (ozone/UV)	Covalent (gas-phase)	1- Large scale treatment 2- Low cost 3- Highly cross-linked coating 4- No vacuum/high pressure requirements 5- Room temperature process 6- High quality films due to low excitation energy	1- Unable to create hydrophobic coatings 2- Limited control on extent of hydrophilicity 3- Low conversion and deposition rate 4- Destructive method for SWCNT structures	[33, 56, 57]
PICVD (syngas/UV)	Covalent (gas-phase)	1- Potential for large scale treatment 2- Low cost processing (inexpensive monomers and PI) 3- Able to make both hydrophilic and hydrophobic surfaces (various extents) 4- Highly cross-linked coating 5- Low energy consumption 6- Selectivity; high control of the overall process (film properties) due to mono-energetic photons that limit reaction pathways 7- No vacuum/high pressure requirements 8- Room temperature process 9- High quality films due to low excitation energy 10- Increased stability compared to their low-pressure plasma counterparts	1- Low conversion and deposition rate	[27, 28, 58]

2. Materials and Methods

2.1. Materials

Pure SWCNTs (P-SWCNTs) grown by radio frequency induction thermal plasma were purchased from Raymor-NanoIntegris (96.5% w/w, Quebec, Canada). The main impurities remaining in the purchased P-SWCNTs are Fe, Ni, Y and amorphous carbon (as identified by XPS and TEM measurements). Hydrogen peroxide (H_2O_2, 50% (w/w)) and n-hexadecane (≥99%, EMD-Millipore) were purchased from Fisher Scientific (Montreal, Quebec). Ozone was generated by an Ozone Solutions TS-40 ozone generator (20 g/h), with ambient air as the gas source. Syngas (CO and H_2, Air Liquide, chemically pure) and argon (Air Liquide, 99.9%), were used as the functionalization precursors and purging gas, respectively. Two 96 cm-long UVC germicidal lamps (Model T-97505-80, Cole-Parmer Inc) were used for all experimental treatments (main emission peak at 253.7 nm, irradiance of 0.01 W/cm^2 at 3.5 cm, measured with an ILT1700 Radiometer equipped with a SED240 detector from International Light Technologies).

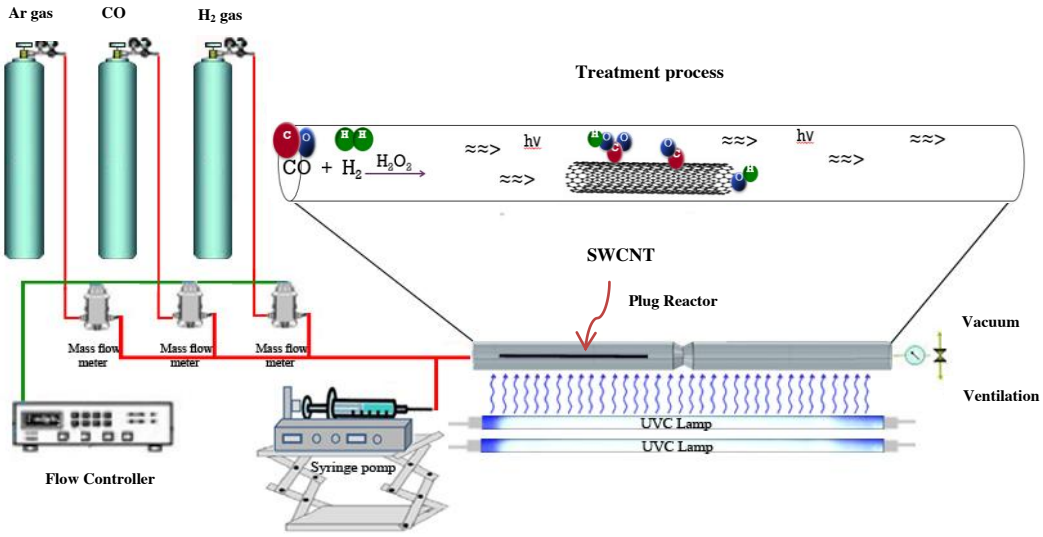

Fig. 1. Schematic of the PICVD setup.

2.2. PICVD Setup

The PICVD reactor used consists of two UVC lamps and a 25-mm internal diameter quartz tube reactor (Fig.1). A syringe pump was used for H_2O_2 injection and Brooks mass flow controllers

(series 5850E) were used to inject precursors (CO and H_2). A centralized vacuum system was applied when working at sub-atmospheric pressure (down to -20 kPa).

2.3. Surface Modification

To modify SWCNT surfaces, the method developed by Dorval Dion et al. (2014) was used [27]. Accordingly, P-SWCNTs (in the form of bucky paper) were placed inside the quartz reactor, which was then closed and sealed. Within the same reactor, SWCNTs were treated with one of two different precursors: ozone or syngas. In the case of ozone treatments, the reactor was purged for two minutes with argon at a rate of 3 L/min then connected to the ozone generator. Ozonated air (5-7% w/w ozone, 500 ml/min) was fed to the reactor under different conditions presented in Table 2. In Table 2, experimental treatments 2 to 6 are related to the SWCNTs treated by ozone/UV while experiments 7 to 27 are dedicated to investigating the effects of treatment time, pressure, position of samples inside the reactor and hydrogen peroxide injection. In the case of syngas/PICVD treatments, the reactor was also purged with argon, then CO and H_2 precursors (total flow rate of 350 ml/min) were introduced at various ratios and conditions, as per Table 2. H_2O_2 was injected simultaneously via the syringe pump as a radical photo-initiator (PI) at a rate of 1 µL/s, directly into the syngas stream. Each experimental treatment was repeated at least 3 times. Six independent variables, including precursor molar ratio (H_2/CO), pressure, treatment time, flow rate of precursors and use of PI and position of samples inside the reactor were studied. According to the desired surface functionality, the process can be operated under slight pressure (up to +15 kPa) or slight vacuum (down to -20 kPa). Hydrophilic surfaces are typically obtained under slight vacuum, using hydrogen peroxide, and near the reactor inlet (16 cm), while hydrophobic surfaces are achieved under pressure closer to the outlet (82 cm), based on previous work performed with copper [27]. During treatment, the surface temperature was monitored using an IR Infrared thermometer. Treatment started at room temperature (~25 °C). Upon activating the UVC lamps, the temperature increased to ~52 °C over the first 15 min, and remained constant until the end of treatment (temperature increase attributable to heat emission from the UVC lamps).

Table 2. Experimental treatment conditions with corresponding wettability (contact angle/surface energy)

Samples		Experimental Conditions						Characterization	
Number	**Description**	**Ratio (H_2/CO)**	**H_2O_2**	**Time (min)**	**Pressure (kPa)**	**Location (cm)**	**Flow Rate (ml/min)**	**Average Contact Angle**	**Surface Energy (mN/m)**
1	n/a	purified	-	-	-	-	500	79±2 °	31
2	ozone/UV	ozone	Yes	60	-20	14	500	< 5°	73
3	ozone/UV	ozone	No	30	-10	14	500	< 5°	73
4	ozone/UV	ozone	Yes	75	-10	82	500	< 5°	73
5	ozone/UV	ozone	Yes	60	+15	14	500	< 5°	73
6	ozone/UV	ozone	No	60	+15	82	500	< 5°	73
7	syngas/PICVD	0.12	Yes	180	-15	14	350	0±3 °	73
8	syngas/PICVD	0.12	No	120	+15	82	350	156±7 °	36
9	syngas/PICVD	0.12	Yes	60	-15	14	350	31±2 °	64
10	syngas/PICVD	0.12	Yes	90	-15	14	350	25±5 °	67
11	syngas/PICVD	0.12	Yes	120	-15	14	350	5±3 °	72
12	syngas/PICVD	0.12	Yes	180	-15	14	350	0±3 °	73
13	syngas/PICVD	0.6	Yes	60	-15	14	350	29±1 °	65
14	syngas/PICVD	1	Yes	60	-15	14	350	47±5 °	54
15	syngas/PICVD	2	Yes	60	-15	14	350	36±3 °	60
16	syngas/PICVD	3	Yes	60	-15	14	350	59±4 °	45
17	syngas/PICVD	0.16	Yes	60	-15	14	350	22±3 °	68
18	syngas/PICVD	0.16	Yes	60	-15	14	300	27±3°	65
19	syngas/PICVD	0.16	Yes	120	-15	14	350	4±7 °	73
20	syngas/PICVD	0.16	Yes	60	-15	14	400	49±2 °	52
21	syngas/PICVD	2	Yes	120	-15	14	350	15+3 °	70
22	syngas/PICVD	0.12	Yes	120	+15	82	350	127± 5°	29
23	syngas/PICVD	0.12	No	120	-15	82	350	93± 6°	26
24	syngas/PICVD	0.12	No	120	+15	14	350	58± 4°	44
25	syngas/PICVD	0.12	No	60	+15	82	350	141± 6°	33
26	syngas/PICVD	2	Yes	120	+15	82	350	135± 3°	31
27	syngas/PICVD	3	No	120	-15	82	350	115± 2°	27

2.4. Surface Characterization

X-ray photoelectron spectroscopy (XPS) was performed with a VG ESCALAB 3 MKII system using Mg Kα x-rays, with a pass energy of 100 eV and energy step size of 1 eV for survey scans. High-resolution (HR) spectra of treated SWCNT (T-SWCNT) buckypapers were obtained at a pass energy of 20 eV, in increments of 0.05 eV. Some of the XPS characterizations were also performed by Kratos Ultra DLD system with a pass energy of 160 eV and step size of 1 eV for survey scans and a pass energy of 20 eV and step size of 0.05 eV for HR spectra, using Al Kα x-rays. Peak fitting was performed as described by Yang and Sacher [59], using the Wagner table for sensitivity factors. Background correction was based on the Shirley method, used within the Thermo Avantage (V4.12) software package. Chamber pressure was kept 5 x 10^{-9} torr.

Surface wetting was assessed through sessile drop contact angle (CA) measurements using a FDS OCA DataPhysics TBU 90E tensiometer. 2 µL droplets of water (as a polar liquid) or n-hexadecane (as a nonpolar liquid) were deposited on 3 different areas of the samples, 3 successive times, in order to obtain the average CA. The exposure time between the droplet and the surface was considered 3 s for all experimental treatments. The surface energy was obtained by applying the Owens-Wendt method (**Equation 1**) to CA measurements (θ_w) with the two different liquids (water/polar and n-hexadecane/nonpolar) [60]. The total free surface energy (γ_s) was obtained by gathering the polar (γ_s^p) and dispersive (γ_s^d) components based on **Equation 2**. Table S1 in supplementary results presents the related information of the liquids.

$$\boldsymbol{\gamma_{sl}(1+cos\theta_w)/2 = \left(\gamma_s^d \gamma_l^d\right)^{0.5} + \left(\gamma_s^p \gamma_l^p\right)^{0.5}} \quad (1)$$

$$\boldsymbol{\gamma_s = \gamma_s^p + \gamma_s^d} \quad (2)$$

Where γ_{sl}, γ_l^d and γ_l^p are the solid-liquid interfacial energy, the total dispersive component and the polar component of liquid surface tension, respectively.

Transmission electron microscopy (TEM, JEOL model JEM2100F) was used to investigate the effect of treatment on SWCNT morphology. The TEM grids used were coated with a lacey carbon film (D20045 grids with formwar substrates, Ni mesh 400, SOQUELEC International). To collect samples, T-SWCNTs were dispersed in methanol at a concentration of 1 mg/mL; TEM grids were then briefly dipped in this suspension (~ 1 s) and analyzed after drying.

The integrity of SWCNT samples was assessed by Raman spectroscopy using a Renishaw Invia Reflex Raman microscope equipped with an argon laser (514 nm), scanning in the range of 300-3500 cm^{-1}. Peak deconvolution was completed through the Renishaw Wire 3.4 software. Gaussian and Lorentzian line shapes were employed for all G′ and D′ bands, respectively, as this combination provides appropriate fits for Raman bands, especially to identify disorder in SWCNTs [61].

Thermal stability was assessed through thermogravimetric analysis (TGA, Model Q500, TA instruments) under air atmosphere. The temperature range was 30-800 °C, with a heating rate of 10 °C/min for all samples. All experimental treatments were carried out with a platinum TGA pan (4 to 5 mg).

3. Results and discussion

3.1. Physical Characterization

To analyse the efficiency of ozone/UV and syngas/PICVD treatments on SWCNTs, we have first determined the physical properties of the treated samples. Table 2 presents the experimental conditions, related water contact angle and surface energy results for ozone/UV and syngas/PICVD treatments. The average water CA of P-SWCNT samples was 79±2° (Fig. 2A). For all SWCNTs treated by ozone/UV (Experimental treatments 2-6), the water CA was <5° (below the detection limit of the instrument), irrespective of treatment time, pressure or position (Fig. 2B). This behavior is expected: ozone peak absorption overlaps with that of the UVC lamps used [62]. These results are consistent with those of Wang et al. (2010), where they showed that ozone/UV treatments of vertically aligned multi-walled carbon nanotubes for 5 min could lead to superhydrophilic surface behavior (reactor operating with 0.2 L/min flow of oxygen gas supply at 50 °C) [62]. Since the peak absorption cross section of ozone is found at 253.7 nm, treatments under UVC light (λ = 200 to 300 nm) cause it to break down into oxygen gas (O_2) and reactive O radicals. These can react with defects sites (or dangling bonds) on the P-SWCNT surface, leading to the formation of -COOH, OH, and CO groups [62]. While ozone/UV allow for the possibility of sidewall functionalization on SWCNTs, longer ozone/UV treatments can actually destroy the SWCNTs' hexagonal carbon structure [63, 64]. While these experiments and previous works show ozone/UV's ability to produce superhydrophilic SWCNT surfaces [62, 65], it highlights its inability to vary surface energy over a wide range even by changing effective parameters such as treatment time, pressure and position inside the reactor (Experimental treatment 2 to 6).

Syngas/PICVD, on the other hand, can generate superhydrophilic surfaces (Table 2, treatment 7, CA<5°, Fig. 2C), all the way to superhydrophobic (Table 2, treatment 8, CA>150°, Fig. 2D), mainly by varying sample position from 14 to 82 cm, treatment pressure from -15 to +15 kPa and absence of hydrogen peroxide as PI. The key parameters influencing hydrophobicity are pressure and location. These are illustrated by comparing treatment 8 and 23: save for pressure, both experiments have the same conditions – a lower pressure (- 15 kPa) leads to more hydrophilic behavior. Similarly, experiment 24, compared to experiment 8, changes only location, showing that positioning the sample closer to the inlet results in hydrophilic behavior. The effect of position can be attributed to the accessibility of syngas-derived radicals, activated monomers and PI-derived species (like OH*) in the reactor [27, 66], while treatment pressure affects the organic chain growth rate and collisions between species and substrate surfaces [27, 67-69]. These effects can also be adjusted to allow intermediate properties to be achieved (Table 2). Moreover, our findings based on tensiometry

characterization show that H_2O_2 addition tends to make surfaces more hydrophilic, given that it photo-dissociates under UVC light (peak between 180 and 200 nm) to generate two hydroxyl radicals (OH•) that can actively participate in the radical-driven syngas and form additional oxygen-containing (hydrophilic) groups [27, 34].

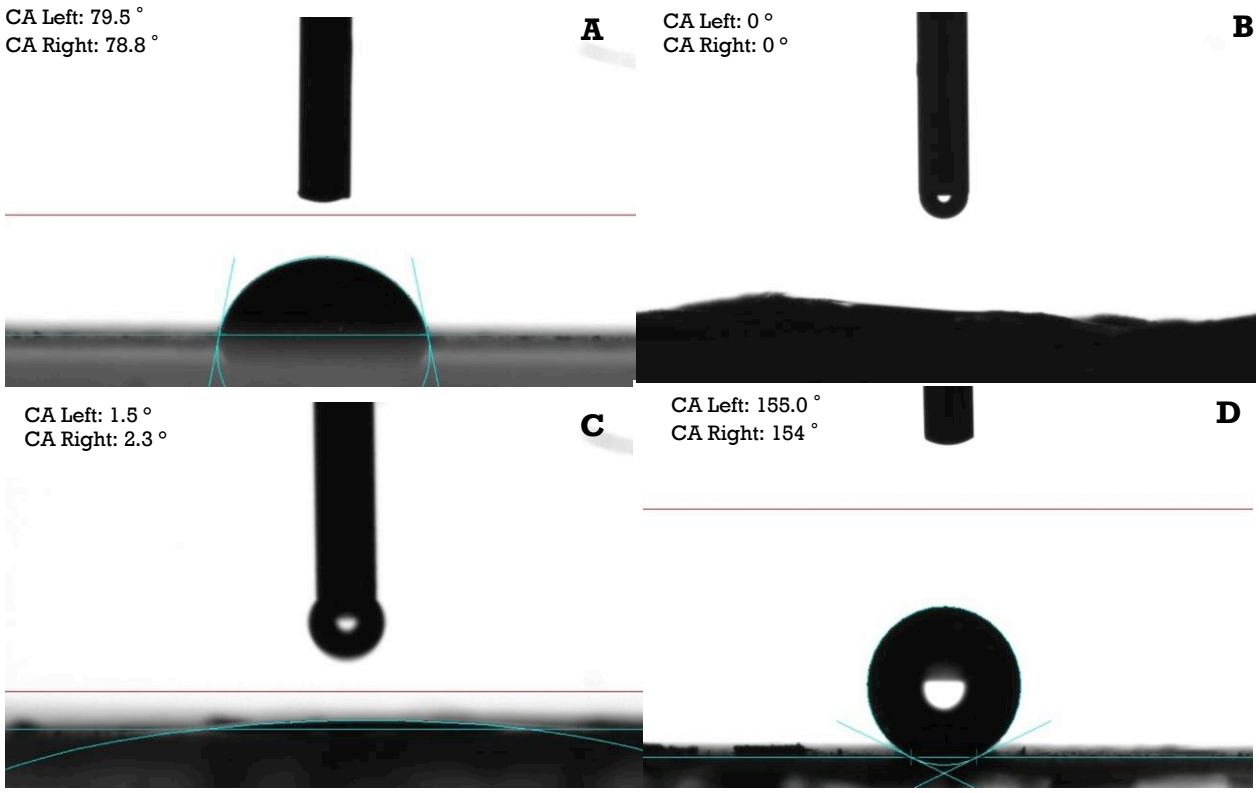

Fig. 2. CA measurement obtained by tensiometry A) P-SWCNT (Experimental treatment 1), B) SWCNTs treated by ozone/UV for 1h (Experimental treatment 2), C) SWCNTs treated by syngas/PICVD under vacuum for 3h (Experimental treatment 7), D) SWCNTs treated by syngas/PICVD under pressure for 2h (Experimental treatment 8).

Experimental treatments 9 to 12 (Table 2) show that SWCNTs become more hydrophilic as a function of treatment time (from 31° at 60 min to 0° at 180 min), likely as a result of additional functional group deposition. Experimental treatments 9, 13 to 17, show that the H_2/CO molar ratio plays a significant role in the syngas/PICVD treatment ($p<0.05$). Indeed, molar ratio is known to play a significant role in binary precursor systems [10, 48, 56, 70]. Several authors used binary mixtures consisting of an oxygen-containing monomers (e.g. O_2 or N_2O) and a hydrocarbon (e.g. CH_4 or C_2H_4) to treat SWCNTs [10, 48, 56, 70] and showed that the concentration of certain functionalities (mostly hydroxyl, carbonyl and carboxylic acid groups) can increase along with an increase in the ratio of oxygen- or nitrogen-containing precursors to hydrocarbons. Fig. 3 shows

that the CA of SWCNTs treated by syngas/PICVD (experimental treatments of 13 to 17 in addition to experimental treatments 9) generally increase as a function of the molar ratio (H_2/CO), likely because fewer oxygen-containing groups are present to increase wetting as the ratio increases. This is confirmed with the overlaid surface tension results. The experimental treatments in Fig. 3 are performed at a constant pressure and reactor position – varying these parameters in combination with molar ratio allows for a full range of surface energies to be attained ranging from 0 ◦ to 156 ◦ (Table 2).

Beyond monomer ratio, our results show that total flow rate in the PICVD reactor can play a role in the final surface properties, given that it will impact residence time in the reactor and, therefore, the probability of collisions between the radicals and the substrate. Except for experimental treatments 18 and 20, all treatments were performed with a total flow rate of 350 ml/min. These two experimental treatments (at 300 and 400 mL/min, respectively), when compared to experiment 17, served to investigate the effect of flow rate. Both experimental treatments 18 and 20 yielded CA higher than at the nominal 350 ml/min flow rate (p-value < 0.05), indicating that hybrid effects may be at play – the reaction domain may switch from deficient to efficient regions (similar to the effect of position). The specific effect of residence time is studied by Farhanian et al (2017) [58]. They reported an increase in film thickness as a function of residence time for a syngas/PICVD system treating flat surfaces [58].

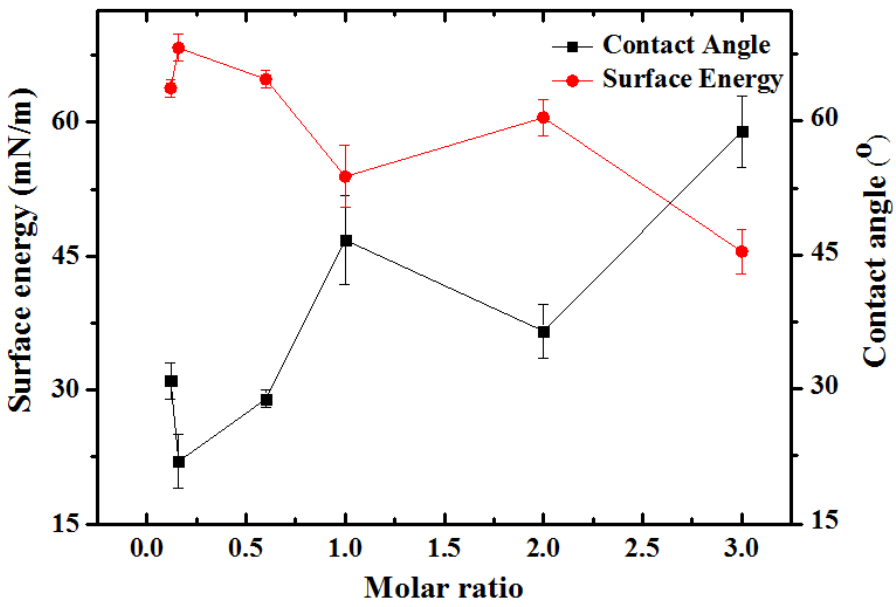

Fig. 3. Black squares: Contact angle measurements of T-SWCNTs obtained by tensiometry in terms of molar ratio of H_2/CO; Red circles: Surface energy measurements that have been plotted in terms of molar ratio. Error bars show standard deviation of three measurements.

It is pertinent to note that the surface energy values presented in Table 2, computed using the Owens-Wendt model (equations 1 and 2), do not consider surface roughness. For this reason, some aberrant values are possible; for example, the surface energy calculated by the tensiometer's software package for experimental treatment 8 (showing superhydrophobic behavior with a contact angle of 156°) is 36 mN/m, nearly unchanged from the far more hydrophilic P-SWCNT (treatment 1, with a contact angle of 79°, 31 mN/m). Given that PICVD treatments on flat surfaces have shown the formation of nanostructured, island-like deposits [58, 71, 72], it is very likely that the increase in roughness plays a large role in the observed wetting behavior.

TEM characterization was done to provide more insight regarding the morphology and structure deposited coatings of T-SWCNTs by syngas/PICVD. Fig. 4 show the morphology of SWCNTs before (A,C) and after (B,D) treatment by syngas/PICVD under slight vacuum (-15 kPa, experimental treatment 11). The principal change observed is the appearance of an apparently polymeric layer on the treated sample. The SWCNT diameter grew from 1.4 nm before treatment to 5.3 nm after treatment.

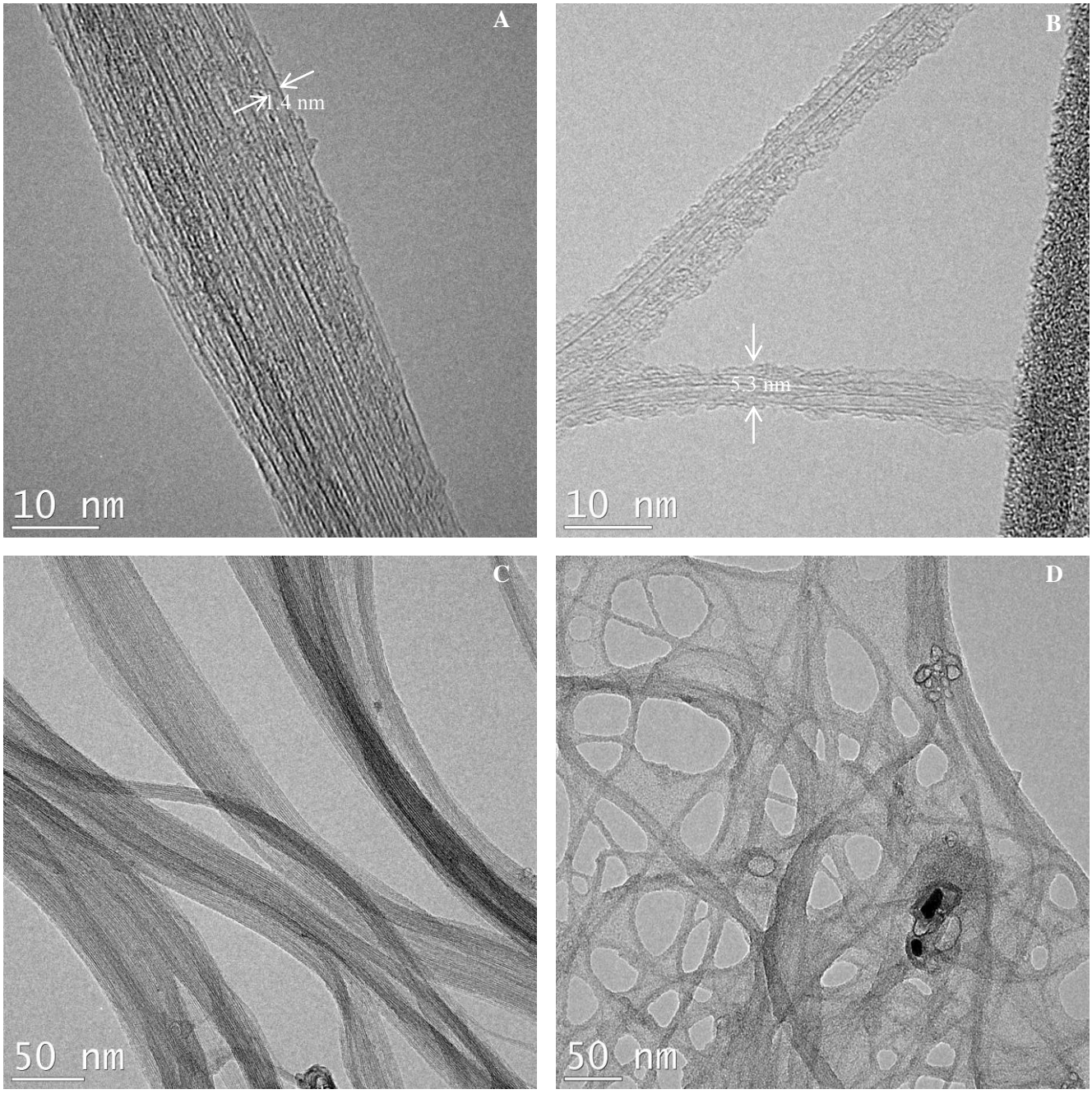

Fig. 4. TEM micrographs of A: P-SWCNTs (Experimental treatment 1), B: Syngas Treated SWCNTs (Experimental treatment 11), C: P-SWCNTs with lower magnification (Experimental treatment 1), D: Syngas treated in lower magnification (Experimental treatment 11).

3.2. Chemical Characterization

We have determined the chemical properties of SWCNTs treated by ozone/UV or syngas/PICVD treatments using XPS. During ozone/UV treatment, the relative oxygen atomic

percentage obtained by XPS survey spectra increased to 20.8% after 30 min (Experimental treatment 3) from untreated P-SWCNTs' 6.9% oxygen content, due to the successful deposition of oxygen-containing groups on the SWCNT surfaces by PICVD (Supplementary Fig. S1) (p-value<0.05). HR-XPS fitting of the C1s peak (Supplementary Fig. S2) shows 6 major functionalities compared to P-SWCNTs: A) 284.6 eV, corresponding to C=C (sp^2); B) 285.7 eV, corresponding to C=C (sp^2) with defects and C–C (sp^3); C) 286.5 eV, assigned to C–O; D) 288 eV, assigned to C=O and $\pi \rightarrow \pi^*$ transition of C=C with defects; E) 289 eV, corresponding to O–C=O; and F) 291.3 eV, assigned to highly delocalized $\pi \rightarrow \pi^*$ transition of C=C [73]. Successful incorporation of oxygen-containing groups (mostly –COOH, C=O and -OH) on the SWCNT surfaces after ozone/UV treatment is confirmed, in agreement with previous studies [57]. Raja et al. (2014) had reported successful incorporation of oxygen-containing groups such as carboxylic acid, hydroxyl and carbonyl groups to SWCNTs while they treated SWCNT under ozone/UV or UV and benzophenone [57]. Experimental treatments 2 to 4 were also used to investigate the effect of treatment time in the case of SWCNTs treated by ozone/UV-treated SWCNT (O-T-SWCNT) by applying 60, 30, and 75 min, respectively. As seen in Supplementary Fig. S3 (inset), oxygen content reaches a plateau ca. 20-26% after 30 min. However, Supplementary Fig. S3 (over plot of C1s HR-XPS spectra of SWCNTs treated by ozone/UV with 60, 30, and 75 min) did not show a significant difference as a function of treatment time. Vautard et al. (2012) reported gas-phase surface treatment of carbon nanofibers in a reactive ozone environment with residence times on the order of 2 min. Their results are in agreement with ours, showing successful incorporation of oxygen-containing groups onto carbon nanofibers [73].

The oxygen content of syngas/PICVD-treated SWCNTs (S-T-SWCNTs, Experimental treatment 1) climbed to 60.1%, with the balance being carbon (18.1%) and iron (21.8%) (Supplementary Fig. S1). The presence of iron (binding energy of 714.4 eV) can be attributed to iron pentacarbonyl ($Fe(CO)_5$) in the CO tank, a common impurity that forms over time in steel tanks exposed to CO; it can readily decompose under the action of heat or UVC light [74]. Fig. 5A and 5B show C1s and O1s HR-XPS spectra of P-SWCNTs to provide comparison with the treated SWCNTs. According to the C1s HR-XPS spectra (Fig. 5C), the syngas-based coating was composed of C-C, hydroxyl (-OH), carboxylic acid (COOH), and carbonate groups, corresponding to binding energies of 285, 286.7, 288.9, and 289.8 eV, respectively. Interestingly, the C1s peak for the treated sample became wider, compared to the untreated sample's more sharp and narrow peak, implying that the coating completely covered the SWCNT surface [75]. Based on the O1s spectra (Fig. 5D), S-T-

SWCNTs have two major peaks at binding energies of 530 and 531.65 eV, which are assigned to O-Fe (or Fe_2O_3) and C-OH, respectively (though $Fe(OH)_3$, phenol and O=C-O-Fe are also possible) [73]. Based on the Fe2p high resolution XPS spectra (Fig. 5E), deposited iron species consisted of Fe_2O_3, FeOOH, and Fe_3O_4 based on peaks at binding energies of 710.55, 713.55, and 718.75 eV, respectively [73]. The Fe_2O_3 and Fe_3O_4 are likely the result of decomposition initiated by the 185 nm peak (as discussed earlier), or through degradation of $Fe(CO)_2$ radicals through collision with reactive species and hydrogen peroxide. Overall, the iron content is essentially in the form of HO-Fe-O, $Fe(OH)_3$ and FeCO due to chemical bond beween iron and carbon.

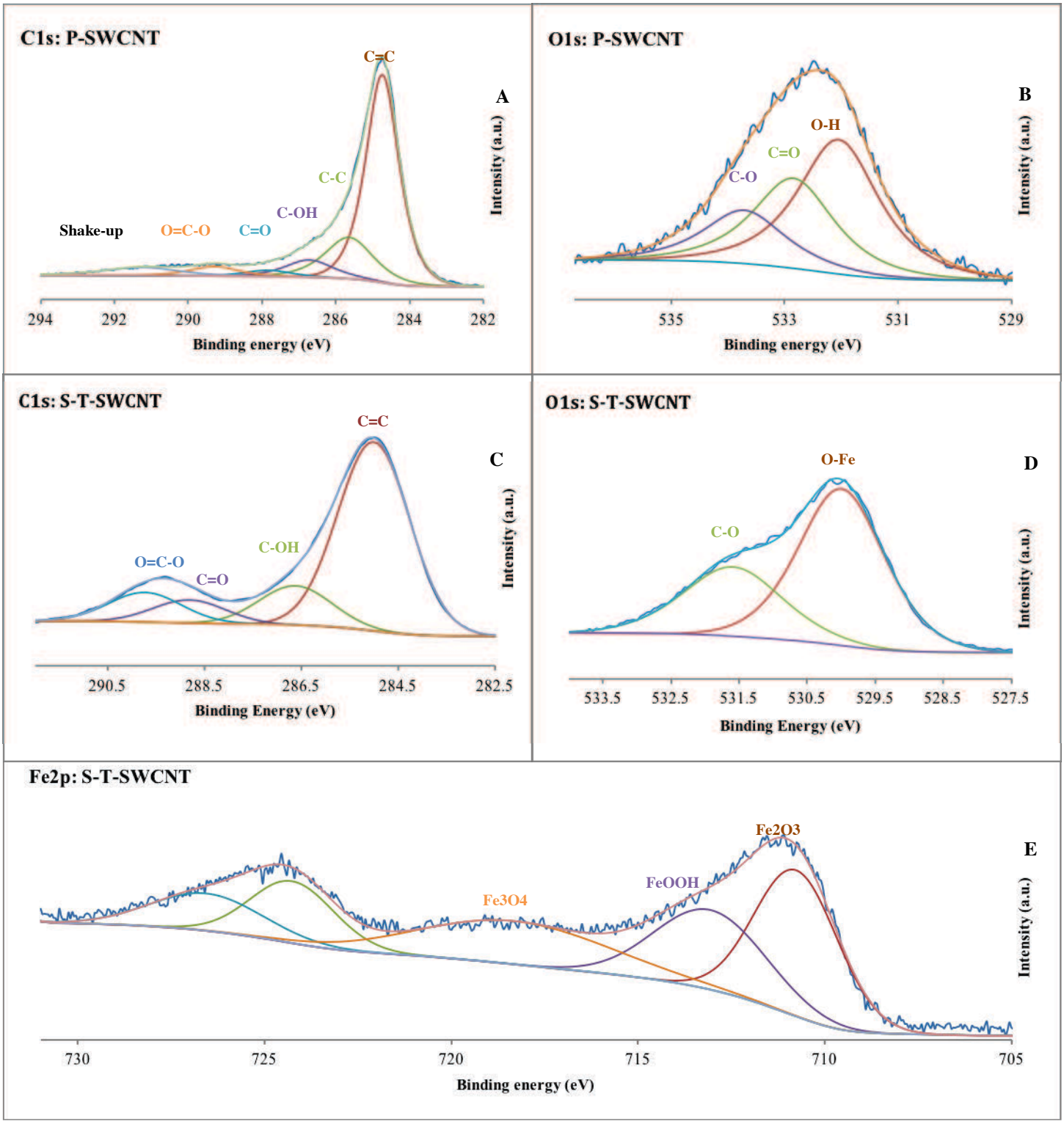

Fig. 5. A: High resolution C1s spectra of P-SWCNT (Experimental treatment 1); B: High resolution O1s spectra of P-SWCNT (Experimental treatment 1); C: High resolution C1s spectra of S-T-SWCNT (Experimental treatment 11); D: High resolution O1s spectra of Treated SWCNT (Experimental treatment 11); E: High resolution Fe2P spectra of T-SWCNT (Experimental treatment 11).

1

To elucidate the role and effect of each individual precursor (H_2, CO, H_2O_2) on coating composition, we performed some blank experiments on glass substrates (thereby eliminating interactions that may occur with SWCNT) (supplementary Table S2). The C1s HR-XPS spectra for bare glass (supplementary Fig. S4A) showed four peaks at binding energies of 285, 286.75, 288.78 and 288.46 eV, assigned to aliphatic carbon or C-C, C-OH and carboxylic acid (COOH) groups, respectively (carbon sourced from airborne contaminants). The O1s spectra (supplementary Fig. S4B) showed two peaks at binding energies of 531.30 and 532.62 eV, corresponding to OH and SiO_2 groups, respectively. After treatment with CO, H_2 and H_2O_2, the same results and structure as those observed on SWCNTs were obtained. Compared to bare glass, the C1s spectra (supplementary Fig. S4C) showed two additional peaks, namely C-Fe and carbonyl groups at binding energies of 284.1 and 290.26 eV, respectively. Moreover, treated glass exhibited decreased hydroxyl groups and significantly increased carboxylic groups. The O1s spectra (supplementary Fig. S4D) showed three new peaks at binding energies of 530.18, 531.67 and 532.61 eV assigned to O-Fe, C-OH groups and O=C-O-Fe, respectively.

In the absence of H_2O_2 (CO and H_2 only), treatment lead to the appearance of two extra peaks compared to bare glass, at binding energies of 284.33 and 289.55 eV (supplementary Fig. S4E). These correspond to C-Fe (or C-Si, as Si could be still seen after treatment in survey peaks), and carbonate groups (adsorbed CO_2), respectively. The spectra are generally similar to the CO+H_2+H_2O_2 case, with increased carboxylic (COOH or COOC) and decreased carbon-bonded hydroxyl groups in the structure. The O1s spectra (supplementary Fig. S4F) also showed three peaks at binding energies of 530.18, 531.67 and 532.61 eV assigned to O-Fe, OH and O=C-O-Fe, respectively. While the chemical differences appear small, the film produced in the absence of H_2O_2 showed significant morphological differences: it appeared as a powder adsorbed on the substrate (not a bound film) and could be removed by shaking lightly. Based on this observation, we can conclude that H_2O_2 plays a determinant role as both a photo-initiator and during film formation.

Knowing that CO can absorb light below 200 nm [27] (including the 185 nm emission peak from the Hg lamps), and that it contains $Fe(CO)_5$, it may lead to deposition without the addition of H_2. When combining CO with H_2O_2 (without hydrogen), the C1s spectra (supplementary Fig. S4G) shows two peaks not present for bare glass at binding energies of 283.9 and 287.3 eV, assigned to C-Fe and C=O, respectively. The peak at binding energy 289.3 eV was also quite significant compared to its bare glass counterpart – it corresponds to carboxylic acid groups bonded to carbon. The O1s spectra

(supplementary Fig. S4H) showed three peaks (530.19, 532.06 and 533.05 eV) assigned to Fe-O (or Fe(OH)O or Fe_3O_4), O-Si and chemisorded H_2O. As expected, combining H_2O_2 with only H_2 lead to no deposit and HR-XPS spectra (supplementary Fig. S4I and S4J) identical to bare glass.

3.3. Thermal Stability and Defects

In order to quantify deposited functionalities on SWCNTs, we performed TGA analyses. Fig. 6 shows TGA and Derivative Thermogravimetric Analysis (DTGA) of P-SWCNTs (experimental treatment 1), S-T-SWCNTs ($CO+H_2+H_2O_2$, experimental treatment 11) and SWCNT exposed to UVC light as a blank experiment. The DTGA graph of P-SWCNT shows two peaks around 618.5 and 542.4 °C, assigned to SWCNTs with sp^2 hybridization and disordered SWCNTs with sp^3 hybridizations, respectively [76]. The P-SWCNTs showed 77.2% carbon with sp^2 hybridization and 14.9% residue which corresponds to metallic and inorganic impurities. There are no significant differences or decomposition shifts between P-SWCNT and SWCNT exposed to UV light. Using the mass loss of P-SWCNTs at 360 °C as a reference (10%), the mass loss of S-T-SWCNTs is about 26%, meaning that treatment leads to decomposition at a lower temperature. This is consistent with previous work where it was shown that a higher amount of functionalities leads to a lower degradation temperature because of more treatment-induced physical defects on the tubes' surfaces and end-caps [57]. The DTGA of S-T-SWCNT shows two new peaks around ca. 113°C and 329°C which are related to oxygen-containing groups and carbon coating on SWCNTs, respectively [77]. The SWCNT peak is also shifted to lower temperatures (from 618.5 to 451.3°C) after treatment (consistent with mass loss results). S-T-SWCNTs presented 0.7% humidity, 19.5% deposited carbon with sp^3 hybridization, 38.7% carbon with sp^2 hybridization and 35% metallic residue. The increase of iron content agrees with XPS results (presence of iron).

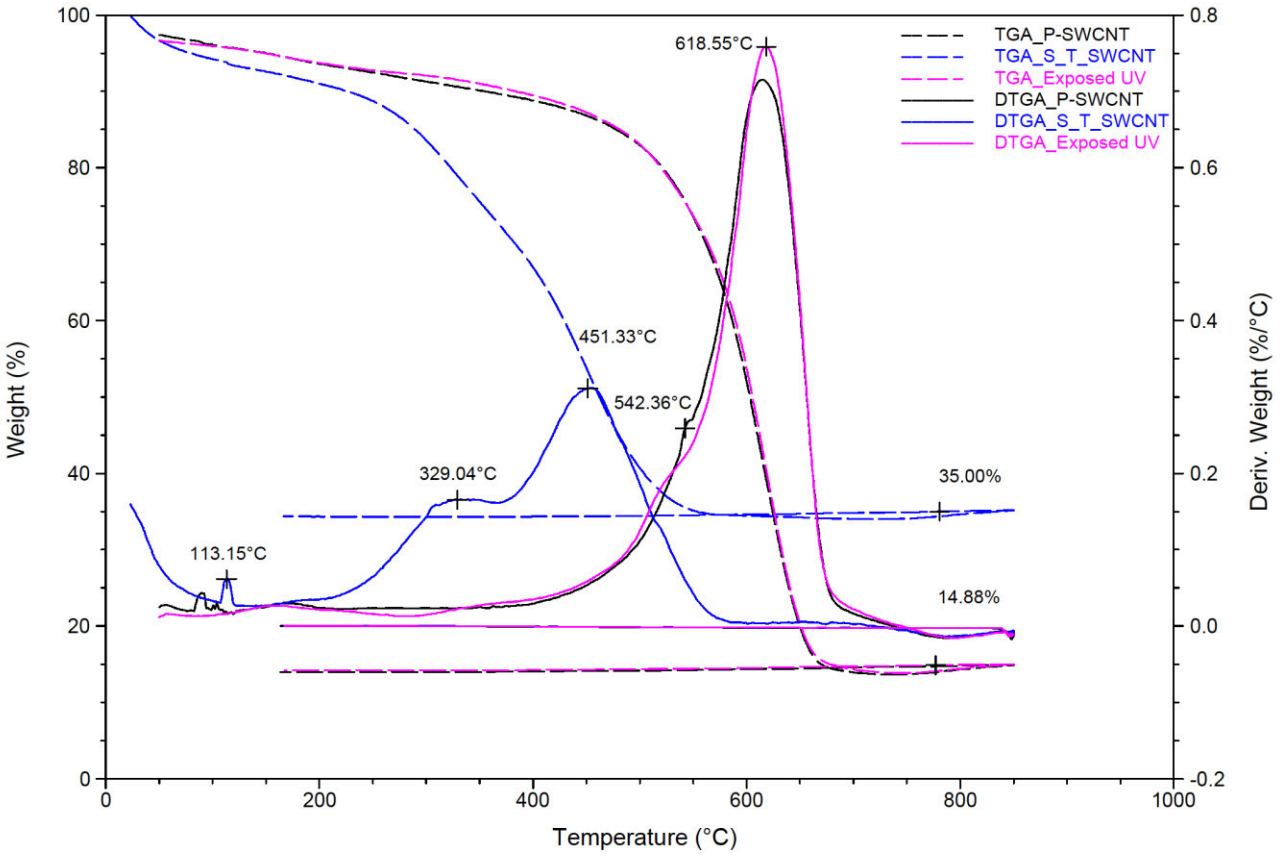

Fig. 6. TGA/DTGA graphs comparing thermal mass loss of P-SWCNTs (Experimental treatment 1), SWCNTs exposed to UV and S-T-SWCNTs treated (Experimental treatment 11).

We characterized T-SWCNTs by Raman spectroscopy to study their hexagonal structure after treatments. Table 3 (extracted from Fig. S5 in supplementary results) shows the Raman spectrum results used to assess SWCNT integrity. The ratio of D- to G-bands in Raman spectra presents defects produced in the hexagonal structure [61]. This ratio is lower for P-SWCNT and increases as a function of treatment time, confirming the tensiometry and XPS findings. If we assume that the D/G ratio is assigned strictly to presence of functionalities producing structural defect sites, the Raman results are also in agreement with the TEM observations (longer treatment leads to a thicker, amorphous carbon coating – from experimental treatment 1 (0 min) to experimental treatment 9 (60 min) to experimental treatment 11 (120 min) to experimental treatment 12 (180 min)) [10]. In the case of 2h treatments, two different molar ratios, namely 0.12 and 2, were evaluated (Experiments 11 and 21). The higher molar ratio (Experimental treatment 21) leads to higher D/G ratio, even higher than that of the long treatment time at low ratio (Experimental treatment 12). This could be explained by the fact that increasing the H_2/CO molar ratio leads to an

organic film with a higher amount of saturated carbon (with oxygen carried away, likely in the form of water).

Table 3. D/G band ratio of SWCNTs before and after treatment at different time obtained by Raman spectra

Samples	Related Experimental Treatment	Time (h)	D/G Bond Ratio
P-SWCNT	1	-	0.29
S-T-SWCNT	9	1	0.34
S-T-SWCNT	11	2	0.36
S-T-SWCNT	12	1	0.43
S-T-SWCNT	21	2	0.58

3.4. Treatment Homogeneity and Dispersibility of SWCNTs

Homogeneous treatment of SWCNT buckypapers will be an important factor in many applications, including polymer nanocomposites or sensors, in which unfunctionalizaed areas may deteriorate mechanical and electrical properties and overshadow the SWCNT's performance improvements [78]. We have performed XPS mapping of three typical SWCNT samples to verify homogeneity of surface coatings (Table 4, experimental treatments 1, 9 and 11) at three different regions on the samples (the head/position P1, middle/P2 and end/P3). Carbon, oxygen and iron content is nearly identical at all positions, confirming that the treatment is homogeneous.

Table 4. XPS mapping results and their experimental conditions

Samples		Characterization								
		O1s			C1s			Fe2p		
		P1	P2	P3	P1	P2	P3	P1	P2	P3
Test 1	1	6.4	6.9	6.6	92.7	92	92	-	-	-
	9	11	12	11	85.7	84.6	85.3	2.4	2.4	2.5
	11	20.5	20.8	17.8	67.5	66.4	72.4	10.5	11	8.2
Test 2	9	8	9	7	90	88.4	91.3	0.7	1.1	0.7
	11	19.3	15.4	16.6	70	78.7	75	9	4.6	7.2

However, this homogeneity may not hold over the full thickness of the bucky paper sample used. Given that many biological assays are conducted SWCNTs in suspension, through-the-thickness heterogeneity may be an issue. To evaluate dispersion, samples exhibiting superhydrophilic behaviors (Experimental treatment 11) were dispersed in deionized water at a

concentration of 0.05 g/mL. After sonicating for 60 minutes, the samples were allowed to settle. Untreated SWCNT samples from areas not reached by the PICVD treatment settled out, while treated S-T-SWCNTs remained in suspension (Fig. 7A). Sediments were removed through decantation and the supernatants remained stable for at least 24 h (Fig. 7B). The "supernatant SWCNTs" are the samples that could be used for cytotoxicity assessments before applying them in biomedical devices. Furthermore, the treatment resists sterilization by immersion of the sample container in a boiling water bath for 30 min (variation in CA <5° before and after boiling, data not reported).

Beyond sterilization in suspension, the S-T-SWCNTs exhibited exceptional stability, hydrophobic samples (from experimental treatment 8) remained at 151±2° after 7 days (ambient conditions), while hydrophilic samples (from experimental treatments 11 and 12) increased to 7±4°. This so-called "hydrophobic recovery" of the hydrophilic-treated sample is a well-documented ageing phenomenon, dependent on absorption of contaminations, reorientation and reconstruction of dangling groups on the surface [13, 46]. However, this phenomenon can be significantly reduced in cross-linking modified surfaces [79]. These dispersion assays demonstrate the change in wettability of individual S-T-SWCNT; dispersion into a wide variety of solvents is the focus of on-going work.

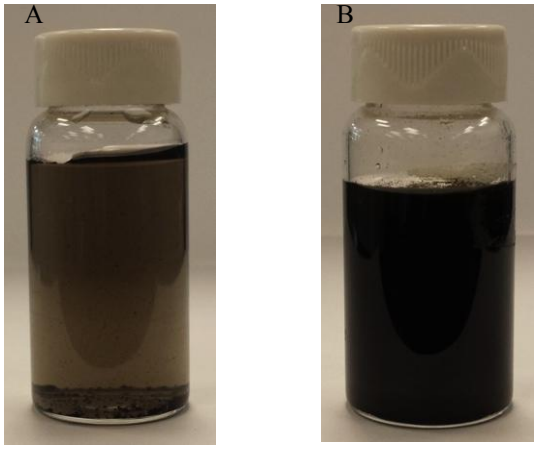

Fig. 7. A) Dispersion of T-SWCNTs in deionized water after 24h, B) Well dispersion of T-SWCNTs under vacuum in deionized water upon treatment.

4. Conclusions

In this study, we compared treatment of SWCNTs by ozone/UV and syngas/PICVD. The main objective of this project was to functionalize SWCNTs with various surface energies ranging from superhydrophilic to superhydrophobic. Although treatment of SWCNTs by ozone/UV was straightforward and superhydrophilic SWCNTs could be obtained in a short time, this method could not meet the main goal of the project. Syngas/PICVD on the other hand provides an efficient method to fabricate functionalized SWCNTs with oxygen-containing groups in a full range of surface energies (ranging from superhydrophilic to superhydrophobic behaviour). Molar ratio of the H_2/CO precursor mix, pressure and treatment time were found to have significant effects during treatment. The PICVD induced coating on the SWCNTs was chemically characterized and proved to be homogeneous (on the surface) and exceptionally stable (including being subjected to boiling for sterilization purposes). This approach is therefore viable as a technique to be used in various applications such as nanocomposites, aerospace and bio applications, in which various degrees of functionality (and consequently surface energies) are desirable. Furthermore, this method will be applicable to investigate the true effect of surface energy on cytotoxicity, which will be the focus of subsequent work.

Acknowledgments

We wish to acknowledge the financial support provided by Fonds de recherche du Québec (FRQNT), as well as moral support from Polytechnique Montreal and Université de Sherbrooke. We would also like also to thank the Université de Sherbrooke Materials Characterization Laboratory, the Polytechnique thin films group (GCM) and the (CM). The authors acknowledge the collaboration of Dr Josianne Lefebvre (Polytechnique Montreal University) for her assistance in analyzing XPS results.

References

[1] M.C. Serrano, M.C. Gutiérrez, F. del Monte, Role of polymers in the design of 3D carbon nanotube-based scaffolds for biomedical applications, Prog. Polym. Sci. 39 (2014) 1448-1471.
[2] E.T. Thostenson, Z.F. Ren, T.W. Chou, Advances in the science and technology of carbon nanotubes and their composites: a review, Compos. Sci. Technol. 61 (2001) 1899-1912.
[3] L.P. Zanello, B. Zhao, H. Hu, R.C. Haddon, Bone cell proliferation on carbon nanotubes, Nano Lett. 6 (2006) 562-567.

[4] P.D. Bradford, A.E. Bogdanovich, Electrical conductivity study of carbon nanotube yarns, 3-D hybrid braids and their composites, J. Compos. Mater. 42 (2008) 1533-1545.
[5] B. Kateb, M. Van Handel, L. Zhang, M.J. Bronikowski, H. Manohara, B. Badie, Internalization of MWCNTs by microglia: possible application in immunotherapy of brain tumors, Neuroimage 37 Suppl 1 (2007) S9-17.
[6] N. Saito, Y. Usui, K. Aoki, N. Narita, M. Shimizu, N. Ogiwara, K. Nakamura, N. Ishigaki, H. Kato, S. Taruta, M. Endo, Carbon nanotubes for biomaterials in contact with bone, Curr Med Chem 15 (2008) 523-527.
[7] J.M. Wernik, S.A. Meguid, Recent Developments in Multifunctional Nanocomposites Using Carbon Nanotubes, Applied Mechanics Reviews 63 (2010) 050801.
[8] Y. Alinejad, N. Faucheux, G. Soucy, Preosteoblasts behavior in contact with single-walled carbon nanotubes synthesized by radio frequency induction thermal plasma using various catalysts, J Appl Toxicol 33 (2013) 1143-1155.
[9] B. Zhao, H. Hu, S.K. Mandal, R.C. Haddon, A bone mimic based on the self-assembly of hydroxyapatite on chemically functionalized single-walled carbon nanotubes, Chem. Mater. 17 (2005) 3235-3241.
[10] J.C. Ruiz, P.L. Girard-Lauriault, F. Truica-Marasescu, M.R. Wertheimer, Plasma- and vacuum-ultraviolet (VUV) photo-polymerisation of N- and O-rich thin films, Radiat. Phys. Chem. 79 (2010) 310-314.
[11] N. Ogihara, Y. Usui, K. Aoki, M. Shimizu, N. Narita, K. Hara, K. Nakamura, N. Ishigaki, S. Takanashi, M. Okamoto, H. Kato, H. Haniu, N. Ogiwara, N. Nakayama, S. Taruta, N. Saito, Biocompatibility and bone tissue compatibility of alumina ceramics reinforced with carbon nanotubes, Nanomedicine : nanotechnology, biology, and medicine 7 (2012) 981-993.
[12] S. Giannona, I. Firkowska, J. Rojas-Chapana, M. Giersig, Vertically aligned carbon nanotubes as cytocompatible material for enhanced adhesion and proliferation of osteoblast-like cells, J. Nanosci. Nanotechnol. 7 (2007) 1679-1683.
[13] Y. Wang, J. Wu, F. Wei, A treatment method to give separated multi-walled carbon nanotubes with high purity, high crystallization and a large aspect ratio, Carbon 41 (2003) 2939-2948.
[14] J. Zhao, Light Scattering Characterization of Carbon Nanotube Dispersions and Reinforcement of Polymer Composites, Department of Chemical and Materials Engineering, University of Cincinnati, 2006.
[15] S. Z hang, T. Shao, S.S. Kaplan-Bekaroglu, T. Karanfil, The Impacts of Aggregation and Surface Chemistry of Carbon Nanotubes on the Adsorption of Synthetic Organic Compounds, Environ. Sci. Technol. 43 (2009) 5719–5725.
[16] M. Foldvari, M. Bagonluri, Carbon nanotubes as functional excipients for nanomedicines: II. Drug delivery and biocompatibility issues, Nanomedicine : nanotechnology, biology, and medicine 4 (2008) 183-200.
[17] Z. Liu, X. Dong, L. Song, H. Zhang, L. Liu, D. Zhu, C. Song, X. Leng, Carboxylation of multiwalled carbon nanotube enhanced its biocompatibility with L02 cells through decreased activation of mitochondrial apoptotic pathway, J Biomed Mater Res A 102 (2014) 665-673.
[18] G. Vuković, A. Marinković, M. Obradović, V. Radmilović, M. Čolić, R. Aleksić, P.S. Uskoković, Synthesis, characterization and cytotoxicity of surface amino-functionalized water-dispersible multi-walled carbon nanotubes, Appl. Surf. Sci. 255 (2009) 8067-8075.
[19] D. Liu, C. Yi, D. Zhang, J. Zhang, M. Yang, Inhibition of proliferation and differentiation of mesenchymal stem cells by carboxylated carbon nanotubes, ACS nano 4 (2010) 2185-2195.
[20] S.L. Montes-Fonseca, E. Orrantia-Borunda, A. Aguilar-Elguezabal, C. Gonzalez Horta, P. Talamas-Rohana, B. Sanchez-Ramirez, Cytotoxicity of functionalized carbon nanotubes in J774A macrophages, Nanomedicine : nanotechnology, biology, and medicine 8 (2012) 853-859.
[21] P. Newman, A. Minett, R. Ellis-Behnke, H. Zreiqat, Carbon nanotubes: their potential and pitfalls for bone tissue regeneration and engineering, Nanomedicine : nanotechnology, biology, and medicine 9 (2013) 1139-1158.
[22] C.B. Dong, A.S. Campell, R. Eldawud, G. Perhinschi, Y. Rojanasakul, C.Z. Dinu, Effects of acid treatment on structure, properties and biocompatibility of carbon nanotubes, Applied Surface Science 264 (2013) 261-268.
[23] S. Vardharajula, S.Z. Ali, P.M. Tiwari, E. Eroglu, K. Vig, V.A. Dennis, S.R. Singh, Functionalized carbon nanotubes: biomedical applications, Int J Nanomedicine 7 (2012) 5361-5374.
[24] C. Ge, J. Du, L. Zhao, L. Wang, Y. Liu, D. Li, Y. Yang, R. Zhou, Y. Zhao, Z. Chai, C. Chen, Binding of blood proteins to carbon nanotubes reduces cytotoxicity, Proceedings of the National Academy of Sciences of the United States of America 108 (2011) 16968-16973.
[25] R.J. Chen, Y. Zhang, D. Wang, H. Dai, Noncovalent sidewall functionalization of single-walled carbon nanotubes for protein immobilization, J. Am. Chem. Soc. 123 (2001) 3838-3839.
[26] Z. Rastian, A.A. Khodadadadi, F. Vahabzade, Y. Mortazavi, Functionalization of Multi -Walled Carbon Nanotubes for Lipase Immobilization, JMTI 1 (2013) 54-71.
[27] C.A. Dorval Dion, W. Raphael, E. Tong, J.R. Tavares, Photo-initiated chemical vapor deposition of thin films using syngas for the functionalization of surfaces at room temperature and near-atmospheric pressure, Surf. Coat. Technol. 244 (2014) 98-108.

[28] C.A. Dorval Dion, J.R. Tavares, Photo-initiated chemical vapor deposition as a scalable particle functionalization technology (a practical review), Powder Technology 239 (2013) 484-491.
[29] K. Balasubramanian, M. Burghard, Chemically functionalized carbon nanotubes, Small 1 (2005) 180-192.
[30] A.H. Lu, E.L. Salabas, F. Schuth, Magnetic nanoparticles: synthesis, protection, functionalization, and application, Angewandte Chemie 46 (2007) 1222-1244.
[31] K.L. Choy, Chemical vapour deposition of coatings, Prog. Mater Sci. 48 (2003) 57-170.
[32] C.A. Dorval Dion, J.R. Tavares, Photo-initiated chemical vapor deposition as a scalable particle functionalization technology (a practical review), Powder Technol. 239 (2013) 484-491.
[33] E. Kasparek, J.R. Tavares, M.R. Wertheimer, P.-L. Girard-Lauriault, Sulfur-Rich Organic Films Deposited by Plasma- and Vacuum-Ultraviolet (VUV) Photo-Polymerization, PLASMA PROCESS POLYM (2016) n/a-n/a.
[34] H. Okabe, Photochemistry of small molecules, Wiley New York1978.
[35] J.Y. Woo, D. Kim, J. Kim, J. Park, C.S. Han, Fast and Efficient Purification for Highly Conductive Transparent Carbon Nanotube Films, Journal of Physical Chemistry C 114 (2010) 19169-19174.
[36] E.P. Koumoulos, C.A. Charitidis, Surface analysis and mechanical behaviour mapping of vertically aligned CNT forest array through nanoindentation, Applied Surface Science 396 (2017) 681-687.
[37] X. Liu, F. Xu, K. Zhang, B. Wei, Z. Gao, Y. Qiu, Characterization of enhanced interfacial bonding between epoxy and plasma functionalized carbon nanotube films, Composites Science and Technology 145 (2017) 114-121.
[38] S. Min, J. Kim, C. Park, J.-H. Jin, N.K. Min, Long-term stability of superhydrophilic oxygen plasma-modified single-walled carbon nanotube network surfaces and the influence on ammonia gas detection, Applied Surface Science 410 (2017) 105-110.
[39] M. Garzia Trulli, E. Sardella, F. Palumbo, G. Palazzo, L.C. Giannossa, A. Mangone, R. Comparelli, S. Musso, P. Favia, Towards highly stable aqueous dispersions of multi-walled carbon nanotubes: the effect of oxygen plasma functionalization, Journal of colloid and interface science 491 (2017) 255-264.
[40] S. Wang, Y. Zhang, N. Abidi, L. Cabrales, Wettability and surface free energy of graphene films, Langmuir 25 (2009) 11078-11081.
[41] A. Paul, POLYMER FUNCTIONALIZED SINGLE-WALLED CARBON NANOTUBE COMPOSITES AND SEMI-FLUORINATED QUATERNARY AMMONIUM POLYMER COLLOIDS AND COATINGS, Oklahoma State University, ProQuest Dissertations, 2012, pp. 194.
[42] M. AfzaliTabar, M. Alaei, R.R. Khojasteh, F. Motiee, A.M. Rashidi, Preference of multi-walled carbon nanotube (MWCNT) to single-walled carbon nanotube (SWCNT) and activated carbon for preparing silica nanohybrid pickering emulsion for chemical enhanced oil recovery (C-EOR), J. Solid State Chem. 245 (2017) 164-173.
[43] B.A. Kakade, V.K. Pillai, Tuning the wetting properties of multiwalled carbon nanotubes by surface functionalization, Journal of Physical Chemistry C 112 (2008) 3183-3186.
[44] K.K.S. Lau, J. Bico, K.B.K. Teo, M. Chhowalla, G.A.J. Amaratunga, W.I. Milne, G.H. McKinley, K.K. Gleason, Superhydrophobic carbon nanotube forests, Nano Letters 3 (2003) 1701-1705.
[45] R. Rajkhowa, A. Kafi, Q.T. Zhou, A. Kondor, D.A.V. Morton, X.G. Wang, Relationship between processing, surface energy and bulk properties of ultrafine silk particles, Powder Technology 270 (2015) 112-120.
[46] I.A. Sacui, R.C. Nieuwendaal, D.J. Burnett, S.J. Stranick, M. Jorfi, C. Weder, E.J. Foster, R.T. Olsson, J.W. Gilman, Comparison of the properties of cellulose nanocrystals and cellulose nanofibrils isolated from bacteria, tunicate, and wood processed using acid, enzymatic, mechanical, and oxidative methods, ACS Appl Mater Interfaces 6 (2014) 6127-6138.
[47] Q.X. Li, J.S. Church, M. Naebe, B.L. Fox, Interfacial characterization and reinforcing mechanism of novel carbon nanotube - Carbon fibre hybrid composites, Carbon 109 (2016) 74-86.
[48] L. Vandsburger, E.J. Swanson, J. Tavares, J.L. Meunier, S. Coulombe, Stabilized aqueous dispersion of multi-walled carbon nanotubes obtained by RF glow-discharge treatment, JNR 11 (2009) 1817-1822.
[49] B. White, S. Banerjee, S. O'Brien, N.J. Turro, I.P. Herman, Zeta-potential measurements of surfactant-wrapped individual single-walled carbon nanotubes, Journal of Physical Chemistry C 111 (2007) 13684-13690.
[50] P. Bilalis, D. Katsigiannopoulos, A. Avgeropoulos, G. Sakellariou, Non-covalent functionalization of carbon nanotubes with polymers, Rsc Advances 4 (2014) 2911-2934.
[51] L. Chen, H. Xie, W. Yu, Functionalization Methods of Carbon Nanotubes and Its Applications, Carbon Nanotubes Applications on Electron Devices (2011).
[52] Y.L. Zhao, J.F. Stoddart, Noncovalent functionalization of single-walled carbon nanotubes, Acc. Chem. Res. 42 (2009) 1161-1171.
[53] Q. Chen, L. Dai, M. Gao, S. Huang, A. Mau, Plasma Activation of Carbon Nanotubes for Chemical Modification, J. Phys. Chem. 105 (2001) 618-622.

[54] T. Xu, J. Yang, J. Liu, Q. Fu, Surface modification of multi-walled carbon nanotubes by O2 plasma, Applied Surface Science 253 (2007) 8945-8951.
[55] J.Y. Yook, J. Jun, S. Kwak, Amino functionalization of carbon nanotube surfaces with NH3 plasma treatment, Applied Surface Science 256 (2010) 6941-6944.
[56] P.L. Girard-Lauriault, R. Illgen, J.C. Ruiz, M.R. Wertheimer, W.E.S. Unger, Surface functionalization of graphite and carbon nanotubes by vacuum-ultraviolet photochemical reactions, Appl. Surf. Sci. 258 (2012) 8448-8454.
[57] M. Raja, Surface Modification of Carbon Nanotubes with Combined UV and Ozone Treatments, FULLER NANOTUB CAR N 23 (2014) 11-16.
[58] D. Farhanian, G. De Crescenzo, J.R. Tavares, Kinetics, Chemistry, and Morphology of Syngas Photoinitiated Chemical Vapor Deposition, Langmuir 33 (2017) 1780-1791.
[59] D.Q. Yang, E. Sacher, s-p hybridization in highly oriented pyrolytic graphite and its change on surface modification, as studied by X-ray photoelectron and Raman spectroscopies, Surf. Sci. 504 (2002) 125-137.
[60] L. Yang, Y.W. Li, B.W. Sheldon, T.J. Webster, Altering surface energy of nanocrystalline diamond to control osteoblast responses, J. Mater. Chem. 22 (2012) 205-214.
[61] S.L. Rebelo, A. Guedes, M.E. Szefczyk, A.M. Pereira, J.P. Araujo, C. Freire, Progress in the Raman spectra analysis of covalently functionalized multiwalled carbon nanotubes: unraveling disorder in graphitic materials, Physical chemistry chemical physics : PCCP 18 (2016) 12784-12796.
[62] H.Z. Wang, Z.P. Huang, Q.J. Cai, K. Kulkarni, C.L. Chen, D. Carnahan, Z.F. Ren, Reversible transformation of hydrophobicity and hydrophilicity of aligned carbon nanotube arrays and buckypapers by dry processes, Carbon 48 (2010) 868-875.
[63] S. Banerjee, S.S. Wong, Demonstration of diameter-selective reactivity in the sidewall ozonation of SWNTs by resonance Raman spectroscopy, Nano Lett. 4 (2004) 1445-1450.
[64] S. Banerjee, S.S. Wong, Rational sidewall functionalization and purification of single-walled carbon nanotubes by solution-phase ozonolysis, J. Phys. Chem. B 106 (2002) 12144-12151.
[65] W. Wang, I. Ruiz, I. Lee, F. Zaera, M. Ozkan, C.S. Ozkan, Improved functionality of graphene and carbon nanotube hybrid foam architecture by UV-ozone treatment, Nanoscale 7 (2015) 7045-7050.
[66] N. Inagaki, Plasma surface modification and plasma polymerization, CRC Press1996.
[67] A. Atkinson, Mercury photosensitized reaction of tetrafluoroethylene, Nature 163 (1949) 291.
[68] J. Heicklen, V. Knight, S.A. Greene, Mercury-Photosensitized Oxidation of Tetrafluoroethylene, J. Chem. Phys. 42 (1965) 221.
[69] J.Y. Tsao, UV laser photopolymerization of volatile surface-adsorbed methyl methacrylate, Appl. Phys. Lett. 42 (1983) 997.
[70] F. Truica-Marasescu, S. Pham, M.R. Wertheimer, VUV processing of polymers: Surface modification and deposition of organic thin films, Nucl. Instrum. Methods Phys. Res. B 265 (2007) 31-36.
[71] V. Labonté, A. Marion, N. Virgilio, J.R. Tavares, Gas-Phase Surface Engineering of Polystyrene Beads Used to Challenge Automated Particle Inspection Systems, Ind. Eng. Chem. Res. 55 (2016) 7362-7372.
[72] A. Berard, G.S. Patience, G. Chouinard, J.R. Tavares, Photo Initiated Chemical Vapour Deposition To Increase Polymer Hydrophobicity, Sci. Rep. 6 (2016) 31574.
[73] F. Vautard, S. Ozcan, F. Paulauskas, J.E. Spruiell, H. Meyer, M.J. Lance, Influence of the carbon fiber surface microstructure on the surface chemistry generated by a thermo-chemical surface treatment, Appl. Surf. Sci. 261 (2012) 473-480.
[74] D.V. Reha K. Tepe, Tracey Jacksier, Ramon M. Barnes, Iron pentacarbonyl determination in carbon monoxide, Spectrochimica Acta Part B 54 (1999) 1861-1868.
[75] T. Susi, T. Pichler, P. Ayala, X-ray photoelectron spectroscopy of graphitic carbon nanomaterials doped with heteroatoms, Beilstein J Nanotechnol 6 (2015) 177-192.
[76] F. Li, Y. Wang, D. Wang, F. Wei, Characterization of single-wall carbon nanotubes by N2 adsorption, Carbon 42 (2004) 2375-2383.
[77] K.S. Kim, M. Imris, A. Shahverdi, Y. Alinejad, G. Soucy, Single-Walled Carbon Nanotubes Prepared by Large-Scale Induction Thermal Plasma Process: Synthesis, Characterization, and Purification, J. Phys. Chem. C 113 (2009) 4340-4348.
[78] O. Kanoun, C. Muller, A. Benchirouf, A. Sanli, T.N. Dinh, A. Al-Hamry, L. Bu, C. Gerlach, A. Bouhamed, Flexible carbon nanotube films for high performance strain sensors, Sensors (Basel) 14 (2014) 10042-10071.
[79] J.M. Goddard, J.H. Hotchkiss, Polymer surface modification for the attachment of bioactive compounds, Prog. Polym. Sci. 32 (2007) 698-725.
[80] X.L. Wang, H.Y. Hu, Q. Ye, T.T. Gao, F. Zhou, Q.J. Xue, Superamphiphobic coatings with coralline-like structure enabled by one-step spray of polyurethane/carbon nanotube composites, J. Mater. Chem. 22 (2012) 9624-9631.

Supplementary Results

Sample Preparation (Bucky papers)

15 mg of purified SWCNTs were dispersed in 10 mL of ethanol by bath sonication for 30 minutes (FS110, Fisher Scientific, power level of 135 W). 400 µL of dispersed SWCNTs were immediately deposited upon a glass substrate and placed in a vacuum oven for more than 3 h at a temperature of 100 °C to completely evaporate the ethanol.

Table S1. Interfacial energy, dispersive and polar components of the liquids used for surface energy computations [80]

Liquids	γ_{sl} (mN/m)	γ_s^d (mN/m)	γ_s^p (mN/m)
Deionized water	73±1	22±1	51
n-hexadecane	26±1	26±1	0±1

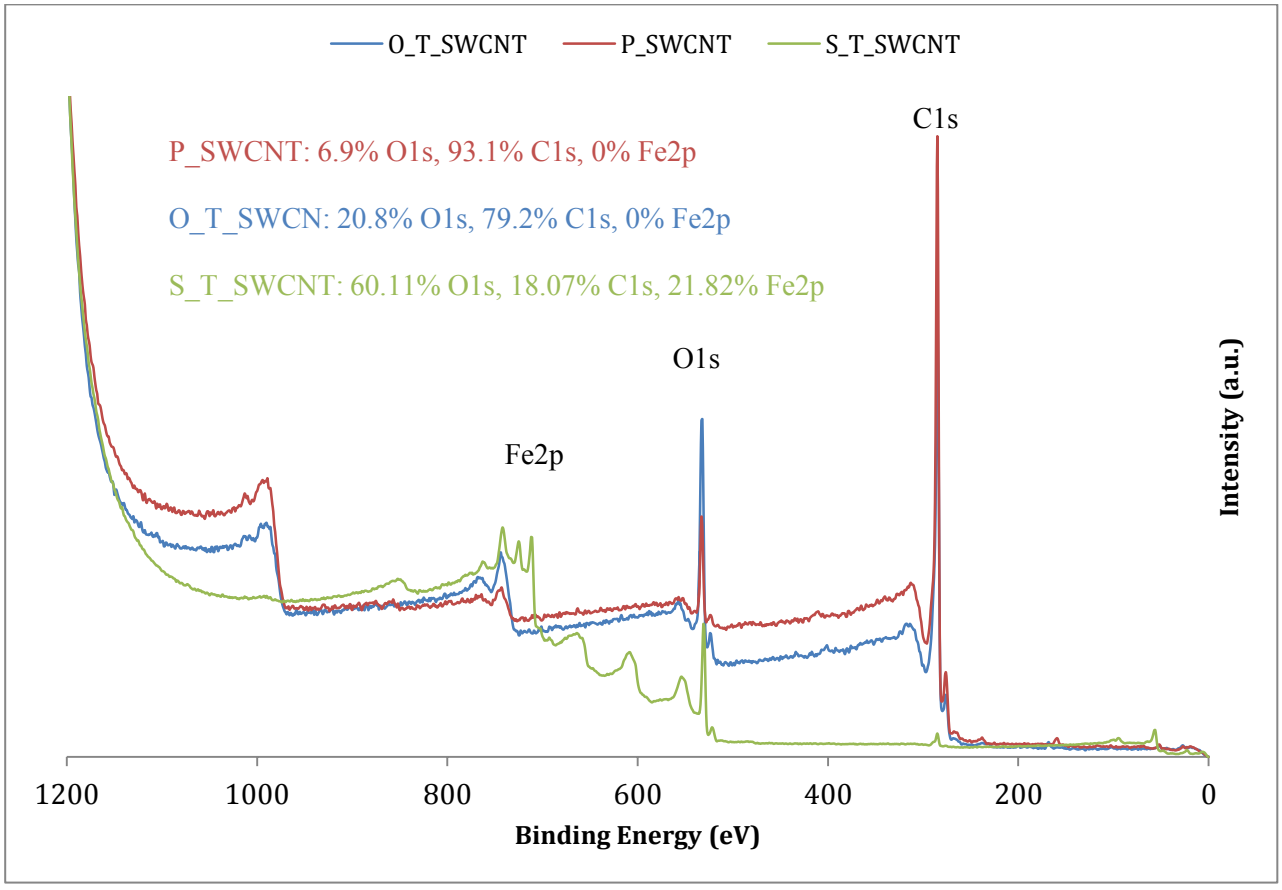

Fig. S1. Survey peaks of S-T-SWCNT after treatment by PICVD

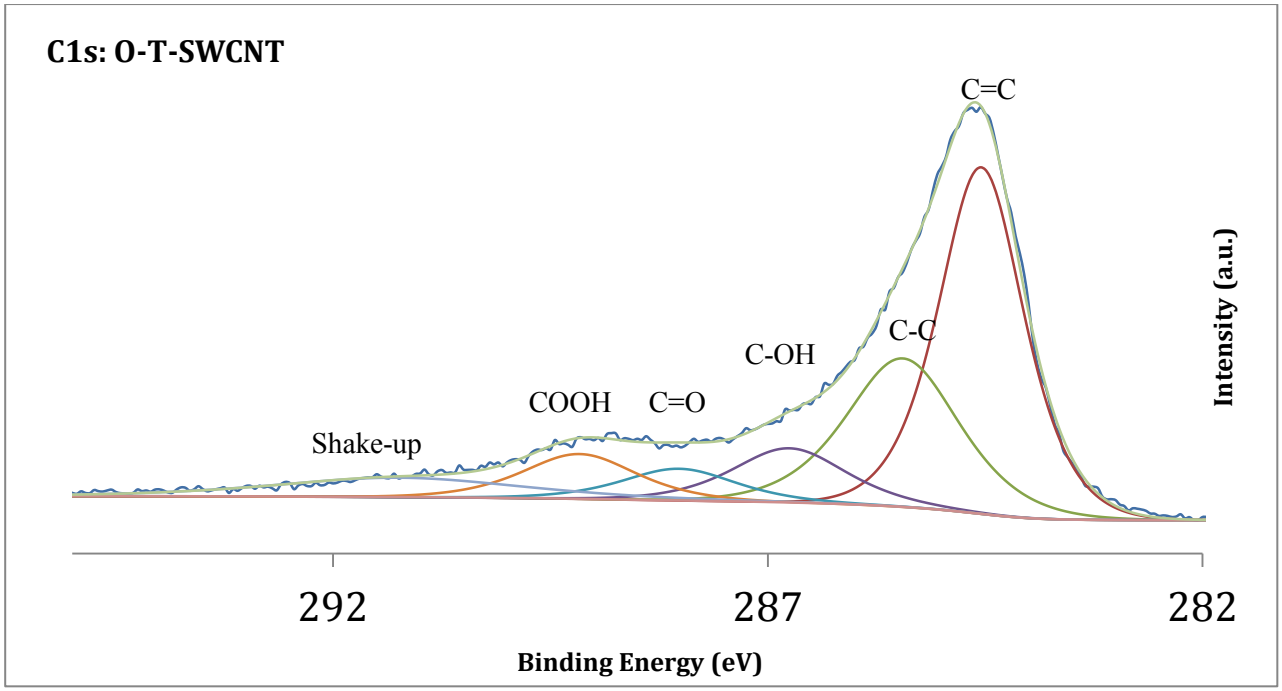

Fig. S2. High resolution XPS spectra of SWCNTs

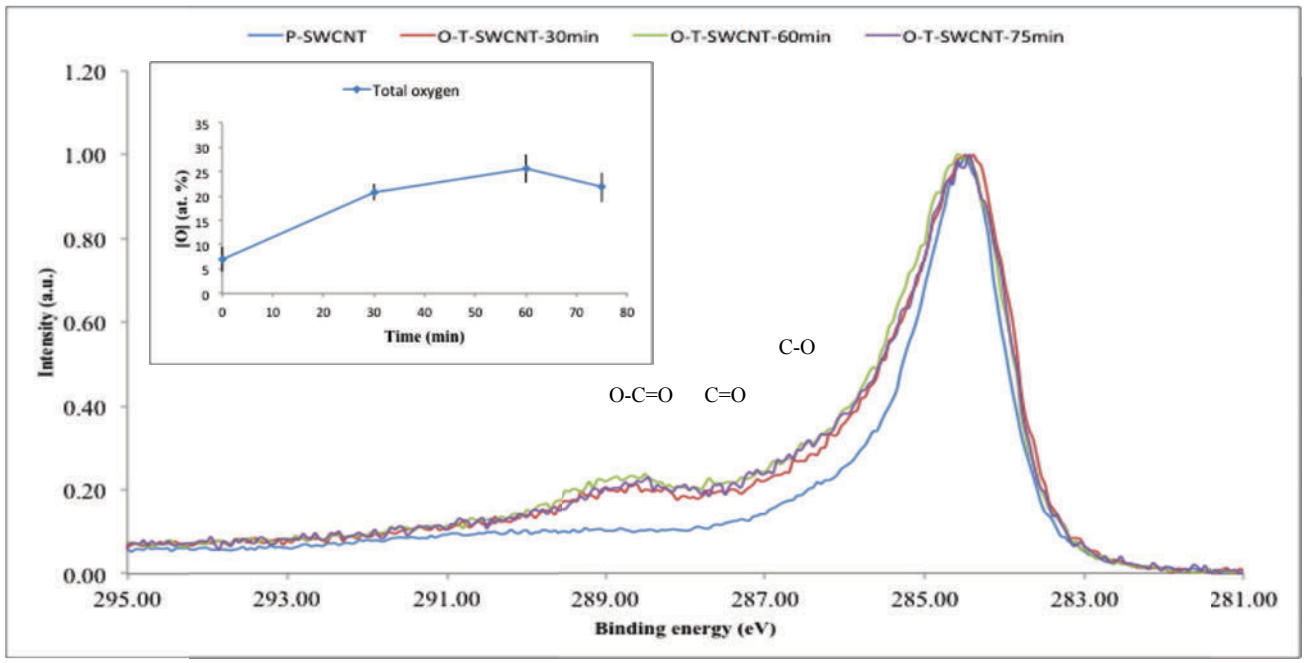

Fig. S3. A) Overlay of C1s XPS spectra, Blue line: ozone/UV treated for 30min, Violet line: ozone/UV SWCNTs treated for 60 min, Red line: P-SWCNTs, Green line: ozone/UV treated for 75 min, Inset: Evolution of survey XPS spectra for ozone/UV SWCNTs in different time (0, 30, 60 and 75 min). Error bars show standard deviation of three measurements.

371 **Table S2.** Blank experiments done based on glass substrates

Conditions	Experimental conditions				
	Pressure (kPa)	**Position (cm)**	**Treatment Time (min)**	**UV**	**Flow (ml/min)**
Glass	n/a	n/a	n/a	n/a	n/a
$CO+H_2+H_2O_2$	0	50	120	Yes	350
$CO+H_2$	0	50	120	Yes	350
$CO+H_2O_2+UV$	0	50	120	Yes	350
$H_2+H_2O_2+UV$	0	50	120	Yes	350

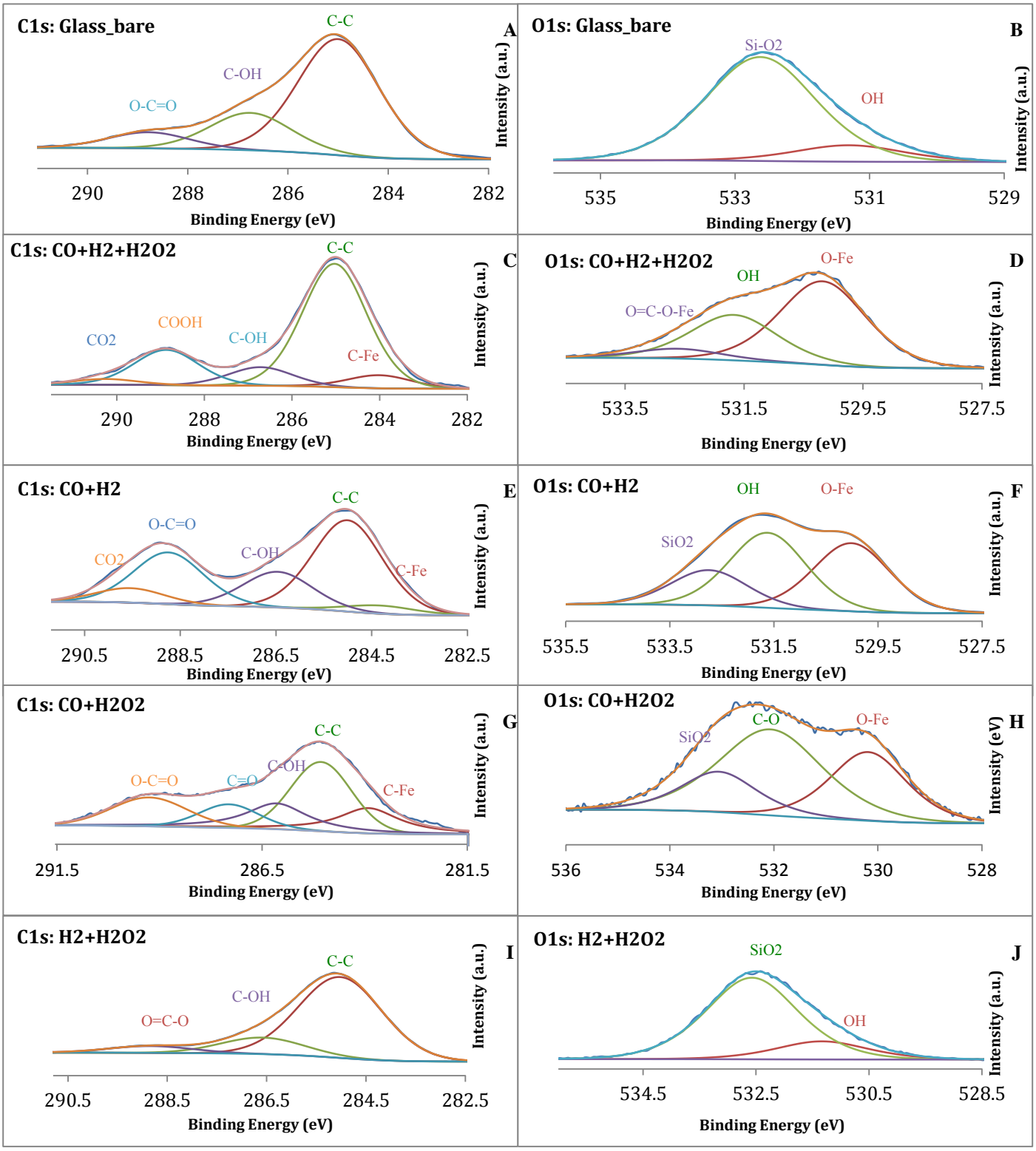

Fig. S4. High resolution spectra of A: C1s for glass (bare); B: O1s for glass (bare); C: C1s for glass treated with $CO+H_2+H_2O_2$; D: O1s for glass treated with $CO+H_2+H_2O_2$; E: C1s for glass treated with $CO+H_2$; F: O1s for glass treated with $CO+H_2$; G: C1s for glass treated with $CO+H_2O_2$; H: O1s for glass treated with $CO+H_2O_2$; I: C1s for glass treated with $H_2+H_2O_2$; J: O1s for glass treated with $H_2+H_2O_2$.

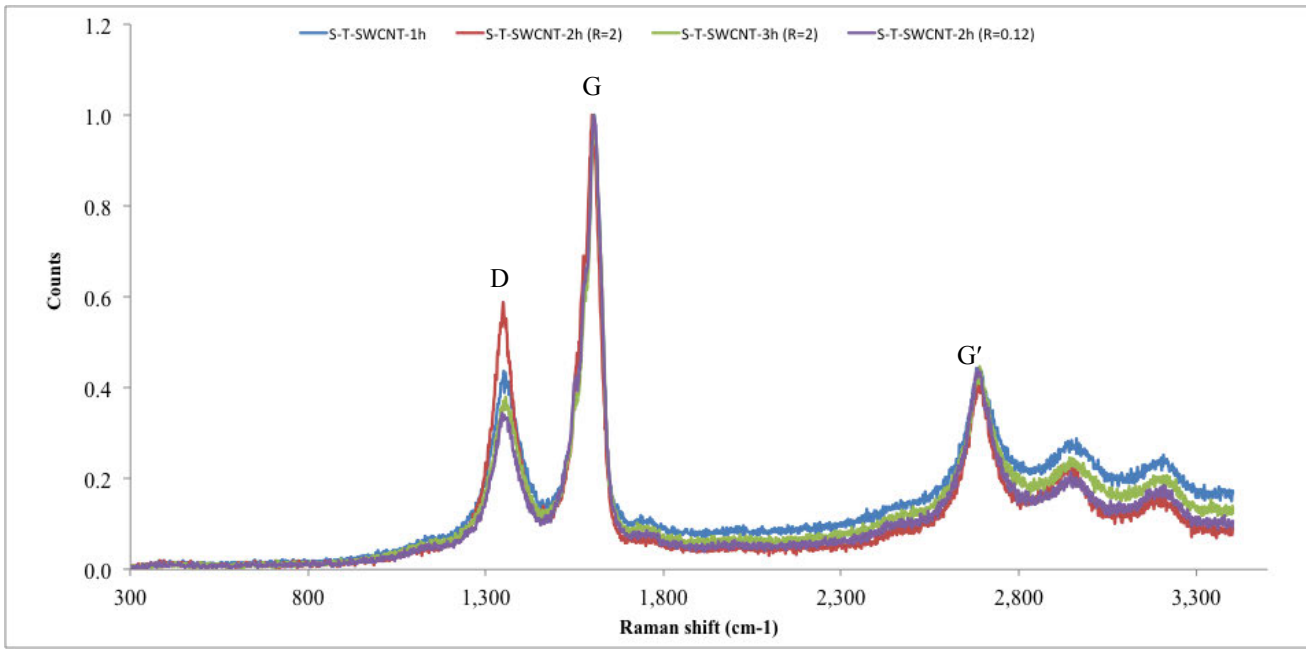

Fig. S5. Wide regions of Raman spectra for the SWCNT materials Light Blue: P-SWCNTs, Violet: T-SWCNTs after 1h and molar ratio of 0.12, Green: T-SWCNTs after 2h and molar ratio of 0.12, Blue: T-SWCNTs after 3h and molar ratio of 0.12. Red: T-SWCNTs after 2h and molar ratio of 2.